

IET Microwaves, Antennas & propagation

Special issue Call for Papers

**Be Seen. Be Cited.
Submit your work to a new
IET special issue**

Connect with researchers and experts in your field and share knowledge.

Be part of the latest research trends, faster.




[Read more](#)



The Institution of
Engineering and Technology

ORIGINAL RESEARCH

Antenna array calibration methods based on simultaneous perturbation

Huijuan Xing¹  | Yongwei Zhang¹  | Yanwei Fu¹  | Xianyang Lv¹ |
Zhihuo Xu¹ | Jiajia Shi¹ | Quan Shi¹ | Murat Temiz² | Ahmed El-Makadema³

¹School of Transportation, Nantong University, Nantong, Jiangsu, China

²Department of Electronic and Electrical Engineering, University College London, London, UK

³Department of Electrical and Electronic Engineering, The University of Manchester, Manchester, UK

Correspondence

Yongwei Zhang, School of Transportation, Nantong University, Nantong, JS 226019, China.
Email: david.y.zhang@ntu.edu.cn

Funding information

Postgraduate Research & Practice Innovation Program of School of Transportation and Civil Engineering, Nantong University, Grant/Award Number: NTUJTXYG12201; National Natural Science Foundation of China, Grant/Award Numbers: 62174091, 62201294; Post-Doc International Exchange Programme, Grant/Award Number: YJ20210098

Abstract

Antenna arrays have gained significant interest in millimetre-wave communication systems as an enabling technology to achieve higher capacity and mitigate the high propagation loss. Such arrays with a large bandwidth need to be efficiently calibrated to maximise their performance. An antenna array calibration method based on a stochastic approximation algorithm and simultaneous perturbation has been developed and the procedures to implement it in both frequency and time domains have been presented. The approaches to define objective functions and establish gradient approximations to fulfill a successful convergence for acquiring calibration coefficients in both domains have been explored. In the time domain implementation, only a fraction of the measurement time was required to calibrate an antenna array of ultrawide bandwidth compared with other methods using a perturbation technique. The effectiveness of the proposed method has been validated via numerical experiments in both domains.

1 | INTRODUCTION

Wideband arrays have become increasingly more imperative in modern mobile communication systems since the 5G and beyond networks operate in multiple frequency bands, that is, 1–6 GHz and the millimeter-wave (mmWave) bands [1]. Furthermore, the number of antenna elements in arrays has been rising to perform massive multiple input multiple output technique [2, 3]. In order to maximise the performance of antenna arrays, the phase of each element has to be calibrated [4–6]. Traditionally, calibration is carried out in the frequency domain, where the radio frequency field in front of the array is physically sampled in half-wavelength increments [7]. This tends to be extremely inefficient for wideband arrays. In particular, for arrays with large apertures, the facilities and techniques involve a significant capital cost and concern practical capability in remote locations.

A variety of algorithms have been developed to calibrate antenna arrays. They are the rotating-element electric-field vector (REV) method [8–10], mutual coupling measurement (MCM) method [11–13], self-calibration method [14–17], and perturbed calibration method [18–20]. All these methods perform phase shift calibration in the frequency domain. It is noted that the REV method is inefficient for large-scale arrays, and the MCM has a strict requirement on isolation between the array elements. Self-calibration is difficult to be implemented in practice as it requires pattern measurements. Calibration through perturbation appears to be more efficient for large-scale antenna arrays with wide frequency bandwidth.

The stochastic approximation (SA) algorithm was used in this study to resolve the phase and time delay deviation caused by imperfect conditions in antenna arrays. The SA algorithm has a significant advantage in the optimisation and estimation of multivariable problems. The corrections of phase shift or

This is an open access article under the terms of the Creative Commons Attribution-NonCommercial License, which permits use, distribution and reproduction in any medium, provided the original work is properly cited and is not used for commercial purposes.

© 2022 The Authors. *IET Microwaves, Antennas & Propagation* published by John Wiley & Sons Ltd on behalf of The Institution of Engineering and Technology.

time delay needed for calibrating can be regarded as the variables in the SA algorithm. There are several perturbation scenarios for the SA algorithm, such as one-side perturbation (1SP), two-side perturbation (2SP), and simultaneous perturbation stochastic approximation (SPSA). These perturbation scenarios achieve different accuracy levels and involve varied complexities. There are M and $2M$ measurements needed in each iteration in the 1SP and 2SP methods, respectively, when M is the number of elements in the antenna array, whereas it only requires two measurements in each iteration using SPSA. All of these methods are effective in multiple variables optimisation. Therefore, the SA algorithm is considered an efficient method and has been widely developed in phased antenna array calibration in the frequency domain.

Perturbation methods are widely applied in searching for gradients from noisy measurements. Cantoni first applied orthogonal perturbation in the calibration of antenna array system [21]. Afterwards, Godara improved the least mean squares algorithm to estimate the required gradients [22]. Both require phase-voltage information, which is difficult to obtain in practice. SA algorithm proposed by Spall can overcome the limitation by estimating the gradients through random perturbations [23–26]. Spall's algorithm makes it more convenient to solve various problems in practice, for example, calibration problems of large phased antenna arrays.

Calibration in the frequency domain requires numerous probe scanning procedures to draw calibration coefficients in a sequential order. To reduce the number of measurements in the frequency domain, Digan further developed the adaptive algorithm for antenna array calibration [19]. The Four-Phase-Cycle (FPC) method has been implemented by Sorace [20] and Wang [27]. More recently, Three-Phase-Cycle has been proposed by Long [28] with only $2M$ (M is the number of elements) measurements required. Comparisons between the methods mentioned above have been listed in the Table 1. Nevertheless, for wideband arrays, the efficiency of calibration in the frequency domain is low, as the value for phase correction obtained from the algorithm is derived from a single frequency and becomes inaccurate for other frequencies.

For large wide band arrays, it is more efficient to perform the calibration in the time domain. This can be achieved by determining the time delay adjustments required to account for all distortions in the channels for all elements. The resolved time delays for calibration can be applied to the whole

frequency band instead of performing the calculation at different frequencies. However, the calibration methods in the time domain are rarely reported due to implementation difficulties involved.

To eliminate distortions of the phase shifts in the frequency domain or incoherent time delays in the time domain, the calibration problem can be turned into seeking optimal values for multiple variables in a system. SA is an effective method to seek the optimal values for multiple variables while the criteria is to reach the minimum value for a customised objective function [25, 29]. A crucial step in the SA algorithm is to make use of the gradient (measured or approximated) of the objective function to move towards the convergence condition. The gradient-free SA algorithm has an advantage, since it only requires the measurement of the objective function, with no need to measure gradients. The adaptive simultaneous perturbation approach is improved by Spall based on the SA algorithm, estimating the required Hessian matrix (or Jacobian matrix) for root finding, making the method more practical [26] than the initial SA algorithm. Furthermore, many approaches have been established to make gradient approximations from measured values of the objective functions that are easier to be obtained. The approximated gradients can be used in three different ways to establish perturbations after mentioned in Refs. [24, 30]. Convergence can be reached for each approach but the total number of measurements needed vary significantly.

The proposed method was based on the SA algorithm with simultaneous perturbation [23, 24], and it has been developed in both frequency and time domains for different applications. The detailed steps were presented and their performances were verified with numerical experiments. One significant advantage of the proposed method is that it needs only two measurements in each iteration despite the number of elements in the array. It is highly promising for large-scale arrays for example, square kilometre array. The successful implementation in the time domain makes it attractive for antenna arrays with a very large frequency bandwidth such as in millimeter and terahertz applications.

In particular, the accuracy level of the methods is strongly dependent on the convergence condition adopted using the objective function at each iteration. The objective functions to apply SA algorithms for antenna array calibration were developed. Two different objective functions were defined to

TABLE 1 Calibration methods based on adaptation or perturbation technique

Phase adaptation	Domain	Measurement	Notes
Adaptive algorithm [18, 31]	Frequency domain	Power	6 (M-1) + 2 measurements
Perturbation algorithm [19]	Frequency domain	Power	6 (M-1) + 1 measurements
FPC(Four-phase-cycle) [20, 27]	Frequency domain	Power	4 (M-1) measurements
Three-phase-cycle [28]	Frequency domain	Amplitude	2M + 1 measurement
MEP(Phase-toggle method) [32, 33]	Frequency domain	Amplitude, phase	M measurements
Fast measurement technique [34]	Frequency domain	Power	7.5 M measurements

Note: M is the total number of elements in the array.

implement the algorithms in frequency and time domains, respectively. In the former case, we calculated the loss function based on power measurement, whereas the correlation coefficient was used for the latter. The strategy to establish the objective functions for a high performance calibration was presented.

This paper is structured as follows: Section 2 describes the basic principle of the SPSA and the specific gradient approximation method for the wideband phased array calibration. Section 3 presents the experiments and results of array calibration in both frequency and time domains. The performance of the proposed method was compared with other calibration methods that involve a perturbation technique. Section 4 summarises the characteristics of the proposed calibration method and gives useful guidelines to implement the method more effectively. Finally, Section 5 concludes this paper.

2 | CALIBRATION METHODS BASED ON PERTURBATION

Calibration is to compensate distortions by seeking optimal coefficients for multiple independent variables in a system. For a system with a single variable, the optimal point is where the derivative of the objective function with respect to the parameter to be optimised is zero. The gradient represents the magnitude of the derivative. Hence, the calculation of the gradient is crucial to locate the optimal point for the objective function. Meanwhile, for some types of situations, such as array calibration, there is no explicit expression to be used to calculate the derivatives. Therefore, the gradients cannot be calculated or measured directly. The approximation of gradients becomes necessary to reach convergence.

Assume $L(x)$ is a continuous function of the variable x , and the derivative concerning x at the point $x = \alpha$, then the function $L(x)$ has the steepest descent at the direction that produces the largest local change in the loss function; hence

$$b = \alpha - \gamma \Delta L(\alpha) \quad (1)$$

where α is a guess value for x , γ is the step size ($\gamma > 0$, often a constant), $\Delta L(\alpha)$ is the derivative of the function $L(x)$ when $x = \alpha$, and b is the new estimate of the best value for x towards the minimum point of $L(x)$.

When $\gamma > 0$ exists, then $L(\alpha) \geq L(b)$, for a series of values for the variable x starting from x_0, x_1, x_2, \dots , which satisfies

$$x_{n+1} = x_n - \gamma \Delta L(x_n) \quad (2)$$

where n is a positive integer, and the following condition becomes true:

$$L(x_0) \geq L(x_1) \geq L(x_2) \geq \dots \quad (3)$$

the $L(x_n)$ tends to converge to its minimum when n increases to a large number. This method, which is based on gradient calculations to find the optimal value, is suitable for a problem

where the expression is known as a function of the variable and there is only one variable to be optimised. But for the question of antenna array calibration, there is a large number of unknown parameters to be determined. Hence, this equation with one variable has to be expanded to include more variables. However, it is difficult to precisely calculate the gradients for many variables in practice. The methods based on gradient approximation (or gradient-free) have been developed to solve the problems. The approximated gradient vector is then introduced as follows:

$$\Delta_V L_k(\cdot) = [\hat{g}_1(k) \hat{g}_2(k) \dots \hat{g}_M(k)] \quad (4)$$

where $\hat{g}_n(k)$ is the estimated partial gradient of $L(\cdot)$ for the n th variable at the k th iteration, and \mathbf{V} represents the vector of parameters to be optimised.

There are mainly three scenarios to establish the approximated gradients for a multivariable problem. The main difference between these three scenarios is how to apply perturbation. In scenario 1, each variable is perturbed separately at each iteration towards one direction, and the gradient is then approximated accordingly, which is called one-side perturbation (1SP). Two-side perturbation (2SP) has been described in scenario 2, and in iterations for optimisation, each variable is perturbed likely in two opposite directions. Compared with the 1SP case, 2SP has a greater perturbation range, hence more measurements are required. In the scenario 3, the simultaneous perturbation is applied incorporating stochastic approximation. In this scenario, all variables vary simultaneously towards two possible directions. A vector Δ , whose elements follow a Bernoulli distribution as positive or negative, determines all perturbation directions for each variable. The equations of gradient approximation for these three scenarios are as follows:

Scenario 1, one-sided gradient estimation:

$$\hat{g}_n(k) = \frac{L(v_1, \dots, v_n(k) \pm \delta, \dots) - L(v_1, \dots, v_n(k), \dots)}{\delta} \quad (5)$$

where k is the iteration number, $v_n(k)$ is the value of the n th variable at the k th iteration, and δ is the coefficient for change.

Scenario 2, two-sided gradient estimation:

$$\hat{g}_n(k) = \frac{L(v_1, \dots, v_n(k) + \delta, \dots) - L(v_1, \dots, v_n(k) - \delta, \dots)}{2\delta} \quad (6)$$

where the value of v_n changes towards two directions at each iteration for gradient approximation.

Scenario 3, gradient estimation based on simultaneous perturbation:

$$\Delta L_k = \frac{L(\mathbf{V} + c_k \Delta_k) - L(\mathbf{V} - c_k \Delta_k)}{2c_k}, \quad (7)$$

where \mathbf{V} is the vector representing the generated values for parameters to be optimised, k is the iteration count, Δ_k is a

vector with M elements and each element is a random number of plus or minus one, and c_k is the magnitude of perturbation at each iteration.

A sequential gradient estimating process is followed in the first two scenarios. Scenario 2 is more stable than scenario 1 to reach convergence successfully; however, $2M$ probes are needed for measurements in the scenario 2, whereas M probes are required in the scenario 1. In order to reduce uncertainty during the long probing process for arrays with a large number of elements, a minimum number of measurements hence shorter period of time for measuring are desired for calibration. Simultaneous perturbation demonstrates its advantage, with only 2 measurements required at each iteration, and thus it takes less time for measurements in each iteration. However, it may potentially need more iterations than the two-sided gradient estimation method to reach convergence. These characteristics are addressed in the following sections.

Figure 1 illustrates the overview diagram on how to apply the SPSA algorithm to solve the array calibration problem. The random phase shift or time delay in each element channel caused by imperfect conditions can be estimated by implementing the proposed method. The phase variation caused by the relative positions of the elements can be calculated according to the direction of arrival of the received signal, the distance between elements, and the frequency. Initially, it is assumed that the element spacing is uniform and the distance between two adjacent elements is d , and d is equal to a half wavelength of the frequency to be calibrated. The angle of arrival is θ off the broadside, so the time delay difference between the element m

and the reference element is $(m-1)d\sin\theta/c$, m is the element number, and c is the speed of light. Accordingly, the phase difference due to element spacing is $2\pi(m-1)d\sin\theta/\lambda$ and λ is the wavelength of the corresponding frequency. The phase shifts or time delays due to element spacing are represented by the vector $\xi = [\xi_1 \ \xi_2 \ \dots \ \xi_M]$, where M is the total number of elements of the array. The vector variable $\gamma = [\gamma_1 \ \gamma_2 \ \dots \ \gamma_M]$ represents the random phase shifts or time delays in the element channels, and they are the values to be calibrated out and unknown to the algorithm. $\tau_1, \tau_2, \dots, \tau_M$ are the values for calibration generated by implementing the SPSA algorithm. At the beginning of the optimisation process, vector $\tau = [\tau_1 \ \tau_2 \ \dots \ \tau_M]$ was generated randomly, and then the τ was renewed in each iteration until the convergence condition was met. The τ generated for the last iteration is considered as the optimal value to cancel the distortions represented by γ . Vectors γ and τ represent phase variations while making calibration in the frequency domain and time delay distortions in the time domain. The array calibration is completed by compensating the distortions represented by γ with the estimated τ^* from the algorithm, and τ^* takes the value of τ when the convergence condition is met. So the objective of the algorithm is to find the optimised values for τ^* , and it consists of approximated values to represent the distortions in the element channels.

The efficacy of implementing the simultaneous perturbation method both in frequency and time domains were evaluated, respectively. In the case of the frequency domain, the random phase shifts in element channels are considered as variables to be optimised. On the other hand, in the time domain, the time delay distortion caused by imperfect receiving conditions is defined as variables to be optimised. The effectiveness of the proposed method was evaluated by comparing the intrinsic random distortions with the approximated values from the algorithm.

2.1 | Simultaneous perturbation stochastic approximation

Simultaneous perturbation stochastic approximation is efficient in optimising multivariable problems. However, it cannot be generalised in a unified form for all possible applications. We adapted the SPSA algorithm to make it viable specifically for antenna array calibration problems as presented in Algorithm 1, and the main steps are summarised as follows:

- Step 1. Initialization and Coefficients Setting: a , c and the convergence threshold. Generate a random vector $\hat{\tau}_k$, let $k = 0$. The updating step of an approximated phase shift or time delay is determined by a , and the range of perturbation is determined by c .
- Step 2. Generation of the Vector for Simultaneous Perturbation: Generate an M -dimensional random perturbation vector, Δ_k ; it is independently generated from a zero-mean probability distribution satisfying the conditions in Ref. [23]. A simple choice for each component of Δ_k is to use a Bernoulli ± 1 distribution with a probability of $1/2$ for each ± 1 outcome.

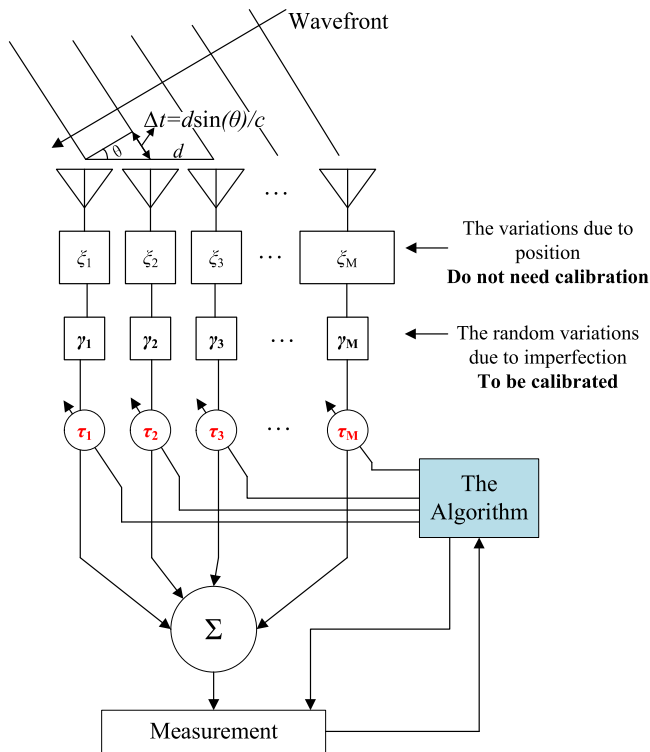


FIGURE 1 Calibration of antenna arrays adopting the simultaneous perturbation technique

- Step 3. Measurement on Loss Function: Obtain two measurements of the loss function $L(\cdot)$ based on the simultaneous perturbation around the $\hat{\mathbf{r}}_k : L(\hat{\mathbf{r}}_k + c\mathbf{\Delta}_k)$ and $L(\hat{\mathbf{r}}_k - c\mathbf{\Delta}_k)$ with the c and $\mathbf{\Delta}_k$ from Step 1 and 2.
- Step 4. Gradient Approximation: Generate the gradient $\hat{\mathbf{g}}_k(\hat{\mathbf{r}}_k)$ based on the simultaneous perturbation:

$$\hat{\mathbf{g}}_k(\hat{\mathbf{r}}_k) = \frac{L(\hat{\mathbf{r}}_k + c\mathbf{\Delta}_k) - L(\hat{\mathbf{r}}_k - c\mathbf{\Delta}_k)}{2c} \begin{bmatrix} \Delta_{k,1}^{-1} \\ \Delta_{k,2}^{-1} \\ \vdots \\ \Delta_{k,M}^{-1} \end{bmatrix} \quad (8)$$

- Step 5. Updating the estimate, $\hat{\mathbf{r}}_k$: Use the standard stochastic approximate form as

$$\hat{\mathbf{r}}_{k+1} = \hat{\mathbf{r}}_k - 2a\hat{\mathbf{g}}_k \quad (9)$$

to renew $\hat{\mathbf{r}}_k$ for the following iteration.

- Step 6. Repeat or Terminate: If the $L(\hat{\mathbf{r}}_k)$ is less than the convergence threshold, terminate the algorithm and let $\mathbf{r}^* \cong \hat{\mathbf{r}}_k$, otherwise go back to Step 2.

In Step 6, \mathbf{r}^* consists of the estimated values from the algorithm and it is used for calibration.

Algorithm 1 Antenna Array Calibration Methods based on Simultaneous Perturbation

Input: parameters M, \mathbf{s}

Output: \mathbf{r}^*

- 1: Assign values to the perturbation constants, a, c and the convergence threshold
- 2: Generate the random variables in channels, γ ; it represented phase shift or time delay distortion in the imperfect channels. It is to be calibrated out using the SPSA algorithm
- 3: Generate the ideal signal while the channels are perfect, S_{peak}
- 4: Measure or calculate the loss function before calibration, L_0
- 5: Make the first guess on the variables in each channel, $\hat{\mathbf{r}}_k$, let $k = 1$
- 6: **while** the loss function $L(\hat{\mathbf{r}}_k)$ does not satisfy the convergence threshold **do**
- 7: Generate the vector for simultaneous perturbation, $\mathbf{\Delta}_k$
- 8: Obtain the measurements $L(\hat{\mathbf{r}}_k + c\mathbf{\Delta}_k)$, $L(\hat{\mathbf{r}}_k - c\mathbf{\Delta}_k)$ respectively
- 9: Calculate the approximated gradient vector for the current loss function

generation in the k th iteration depending on the two measurements $L(\hat{\mathbf{r}}_k + c\mathbf{\Delta}_k)$, $L(\hat{\mathbf{r}}_k - c\mathbf{\Delta}_k)$, the gradient

$$\text{vector is, } \hat{\mathbf{g}}_k(\hat{\mathbf{r}}_k) = \frac{L(\hat{\mathbf{r}}_k + c\mathbf{\Delta}_k) - L(\hat{\mathbf{r}}_k - c\mathbf{\Delta}_k)}{2c} \begin{bmatrix} \Delta_{k,1}^{-1} \\ \Delta_{k,2}^{-1} \\ \vdots \\ \Delta_{k,M}^{-1} \end{bmatrix}$$

- 10: Calculate the variables adjustment matrix for the next iteration, $\hat{\mathbf{r}}_{k+1} = \hat{\mathbf{r}}_k - a\hat{\mathbf{g}}_k(\hat{\mathbf{r}}_k)$, let $k = k + 1$
- 11: **return** Variables offset for each channel, $\mathbf{r}^* \cong \hat{\mathbf{r}}_k$

2.2 | Perturbation in the frequency domain

For a signal of continuous wave impinging on the broadside array with an angle θ off the boresight, the received signals by each element can be expressed as follows:

$$s_m = A_m e^{-i(\xi_m + \gamma_m)} \quad (10)$$

where $\xi_m = 2\pi(m-1)d\sin\theta/\lambda$ is the phase shift for the element number, m , with respect to the reference due to spacing, and the element number $m = 1$ is taken as a reference and its intrinsic phase $\xi_1 = 0$; the spatial phase shifts for the elements are presented as $\xi_2 = 2\pi d\sin\theta/\lambda$, $\xi_3 = 2\pi(2d)\sin\theta/\lambda$, \dots , and $\xi_M = 2\pi(M-1)d\sin\theta/\lambda$. λ is the wavelength, and d is the interelement spacing. γ_m represents the random phase shift generated in the system for the m th element channel and is the distortion to be determined. In (10), A_m represents the gain for the element m , and θ is the angle of arrival off the boresight. The signal received at each element is $s_1 = A_1 e^{-i(\xi_1 + \gamma_1)}$, $s_2 = A_2 e^{-i(\xi_2 + \gamma_2)}$, \dots , $s_M = A_M e^{-i(\xi_M + \gamma_M)}$, and the signals from all elements before combining can be expressed by a vector,

$$\mathbf{s} = [s_1 \quad s_2 \quad \dots \quad s_M]. \quad (11)$$

Phase perturbation is introduced in the signal channel for each element, $\hat{\psi}_{k,1}$, $\hat{\psi}_{k,2}$, \dots , $\hat{\psi}_{k,M}$, k is the iteration number, and the corresponding effects in the element channel can be treated as applying weights before combining in the array receiver, $e^{i\hat{\psi}_{k,1}}$, $e^{i\hat{\psi}_{k,2}}$, \dots , $e^{i\hat{\psi}_{k,M}}$; they can then be represented by

$$\mathbf{w} = [e^{i\hat{\psi}_{k,1}} \quad e^{i\hat{\psi}_{k,2}} \quad \dots \quad e^{i\hat{\psi}_{k,M}}]. \quad (12)$$

And the optimum values of the phases in the channel for correction are realised through iterations indicated by

$$\hat{\psi}_{k+1} = \hat{\psi}_k - 2af\hat{\mathbf{g}}_k, \quad (13)$$

where $\hat{\boldsymbol{\psi}}_k = [\hat{\psi}_{k,1} \hat{\psi}_{k,2} \cdots \hat{\psi}_{k,M}]$ is the phase perturbation introduced in the element channels, the change step of phase in each element channel between adjacent iterations is controlled by the approximated gradient, and $\hat{\mathbf{g}}_k$ is a vector consisting of gradients towards convergence, and at the k th iteration,

$$\hat{\mathbf{g}}_k(\hat{\boldsymbol{\psi}}_k) = \frac{L_f(\hat{\boldsymbol{\psi}}_k + c_f \boldsymbol{\Delta}_k) - L_f(\hat{\boldsymbol{\psi}}_k - c_f \boldsymbol{\Delta}_k)}{2c_f} \begin{bmatrix} \Delta_{k,1}^{-1} \\ \Delta_{k,2}^{-1} \\ \vdots \\ \Delta_{k,M}^{-1} \end{bmatrix}. \quad (14)$$

Therefore, the combined signal at the array output is given by

$$\mathbf{V} = \mathbf{s} \cdot \mathbf{w}^T. \quad (15)$$

The criteria for convergence of the algorithm based on perturbation is to maximise the power at the array output, defined by $P = \mathbb{E}\{|V|^2\}$; this can be achieved by repeating iterations until the convergence condition is satisfied, and the objective function for convergence is defined as follows:

$$L_f = 1 - \frac{P_k}{P_{\text{peak}}}, \quad (16)$$

where the P_k is the measured power of \mathbf{V} , the combined signal at output at the k th iteration, with perturbed phase shifts applied in element channels. P_{peak} is the maximum power of the combined signal at the array output, which is generated in the antenna array with a hypothetically perfect receiving condition. The distinction of the simultaneous perturbation technique compared with other conventional approaches is that the gradients for all channels (represented by the vector, $\hat{\mathbf{g}}$) are all approximated simultaneously instead of in a sequential order.

In each iteration of the algorithm, the value of the loss function, L_f , is renewed and compared against the value assigned as the convergence condition. The iteration loops keep running until the value of L_f meets the convergence condition.

When the loops of the algorithm terminated, the vector $\boldsymbol{\psi}^*$ is obtained and used to compensate the phase shift distortions caused by the devices, temperature, or other factors. A calibrated phased antenna array can be acquired by using the corresponding elements in $\boldsymbol{\psi}^*$ to cancel out the phase distortion in each element channel.

2.3 | Perturbation in the time domain

In the case of time domain, the signal from far field impinging upon the array is assumed as a short pulse, and it is defined as follows [35]:

$$\mathbf{s}(\mathbf{t}) = \frac{1}{4\sqrt{2\pi\sigma_p^2}} e^{-\frac{t^2}{2\sigma_p^2}}, \quad (17)$$

where σ_p^2 denotes the variance of the Gaussian pulse. The signals received by array elements in response to the short pulse with an incidence angle of θ off the boresight direction for a broadside array can be denoted by $\mathbf{s}_1(\mathbf{t}) = \mathbf{s}(\mathbf{t} + \xi_1 + \gamma_1)$, $\mathbf{s}_2(\mathbf{t}) = \mathbf{s}(\mathbf{t} + \xi_2 + \gamma_2)$, \cdots , $\mathbf{s}_M(\mathbf{t}) = \mathbf{s}(\mathbf{t} + \xi_M + \gamma_M)$. M is the number of elements consisted in the antenna array. ξ_m is the time delay for the m th element due to relative distance to the reference element. And the intrinsic time delay, γ_m , represents the random time delay produced in the array system within the m th element channel and is the coefficient to be calibrated out, and m is the antenna element number. Accordingly, the signal received at the m th element before calibration is $\mathbf{s}_m(\mathbf{t}) = A_m e^{-(t+\xi_m+\gamma_m)^2/2\sigma_p^2}$, and A_m is the amplitude of the signal. The generated signal in the k th iteration for the m th element in calibration process can be expressed as follows:

$$\mathbf{s}_m(\mathbf{t}) = A_m e^{-[t+\xi_m+(\gamma_m-\hat{\tau}_{k,m})]^2/2\sigma_p^2}, \quad (18)$$

$\hat{\tau}_{k,m}$ is the perturbed time delay for the m th element channel at the k th iteration, which corresponds to the τ_m in the flow chart indicated in Figure 1, and $\hat{\boldsymbol{\tau}}_k = [\hat{\tau}_{k,1} \hat{\tau}_{k,1} \cdots \hat{\tau}_{k,M}]$. The received signal at the output is the sum of all channels when the $\hat{\boldsymbol{\tau}}_k$ is applied, which can be expressed as follows:

$$\mathbf{s}_k = \sum_{m=1}^M \mathbf{s}_m(\mathbf{t}). \quad (19)$$

The gradient in each iteration is approximated by

$$\hat{\mathbf{g}}_k(\hat{\boldsymbol{\tau}}_k) = \frac{L_t(\hat{\boldsymbol{\tau}}_k + c_t \boldsymbol{\Delta}_k) - L_t(\hat{\boldsymbol{\tau}}_k - c_t \boldsymbol{\Delta}_k)}{2c_t} \begin{bmatrix} \Delta_{k,1}^{-1} \\ \Delta_{k,2}^{-1} \\ \vdots \\ \Delta_{k,M}^{-1} \end{bmatrix}, \quad (20)$$

then the $\hat{\boldsymbol{\tau}}_{k+1}$ is derived according to Equation (9) for the following iteration:

$$\hat{\boldsymbol{\tau}}_{k+1} = \hat{\boldsymbol{\tau}}_k - 2a_t \hat{\mathbf{g}}_k. \quad (21)$$

The loss function for calibration in the k th iteration in the time domain is defined by

$$L_t = 1 - R_k C_k, \quad (22)$$

where R_k and C_k can be respectively calculated by

$$R_k = \frac{P_k}{P_{\text{peak}}}, \quad (23)$$

$$C_k = \frac{\sum_{n=1}^N [\mathbf{s}_k(n) - \bar{\mathbf{s}}_k] [\mathbf{s}_{\text{peak}}(l) - \bar{\mathbf{s}}_{\text{peak}}]}{\sqrt{\sum_{n=1}^N [\mathbf{s}_k(n) - \bar{\mathbf{s}}_k]^2} \sqrt{\sum_{l=1}^N [\mathbf{s}_{\text{peak}}(n) - \bar{\mathbf{s}}_{\text{peak}}]^2}}, \quad (24)$$

where N is the length of \mathbf{s}_k and \mathbf{s}_{peak} , which is determined by the sampling time range T and sampling interval dt , $N = T/dt + 1$. $\bar{\mathbf{s}}_k$ and $\bar{\mathbf{s}}_{\text{peak}}$ represent the means of \mathbf{s}_k and \mathbf{s}_{peak} respectively. \mathbf{s}_{peak} means the measured combined signal at the array output. \mathbf{s}_{peak} denotes the ideal signal without intrinsic time delays and with the maximum output power. R_k is the ratio of the power of \mathbf{s}_k to \mathbf{s}_{peak} , and C_k is the correlation coefficient between \mathbf{s}_k and \mathbf{s}_{peak} . The power of \mathbf{s}_k , P_k , is measured at the output of the antenna array during the calibration, and the power of \mathbf{s}_{peak} , R_k and C_k are calculated.

Once the value of the loss function satisfies the convergence condition, the algorithm terminates. $\boldsymbol{\tau}^*$ takes the values of $\hat{\boldsymbol{\tau}}_k$ from the last iteration, and is used for calibration.

3 | THE EXPERIMENTS AND RESULTS

In order to illustrate how to implement the proposed algorithm in practice, an antenna array consisting of 16 elements was used for the numerical experiments both in frequency and time domains. Two types of signals (continuous wave in the frequency domain and a short pulse in the time domain) were adopted and they were hypothesised impinging on the array with a designated direction of arrival. The arrays for the experiments were in a linear configuration with the element spacing of half a wavelength at 1 GHz. The method can be easily applied to other array configurations as the algorithm deals with random distortions in the system where the fixed changes to the phase shift or time delay associated with array configurations and relative separations were assumed to be known.

3.1 | The experiment in the frequency domain

In the settings for the frequency domain experiment, random phase distortions were introduced in the element channels, and then the algorithm was implemented following the steps presented in Section 2.2. The total number of elements was $M = 16$, and the coefficient constants for the algorithm were chosen as $a_f = 0.001$, and $c_f = 0.05$. The a_f largely determines whether the convergence can be achieved, and the c_f was a factor related to the speed for reaching convergence and accuracy of the algorithm. In this experiment, the a_f was estimated to be 0.001 to ensure a successful convergence; we optimised c_f through recursions and found that $c_f = 0.05$ was the optimum value to fulfill convergence with a minimum number of iterations. The introduced intrinsic phase distortion for the m th element channel, γ_m , was restricted in the range of $[0, 90]$ degree and the vector representing the phase distortions in all element channels, $\boldsymbol{\gamma}$, was generated following the Gaussian distribution: [28.8656, 59.3298, 34.1426, 86.7745, 50.2198, 14.3354, 44.9314, 39.6659, 86.1213, 48.478, 8.2334, 4.3258, 4.3258, 36.3771, 78.2317, 64.1999, 45.3267] degree. On implementing the algorithm, the initial guess on the phase distortions for correction, $\boldsymbol{\gamma}_0$ was generated with its components in the same range and followed the same distribution. The interelement spacing, d , was

half a wavelength at 1 GHz, with the angle of arrival $\theta = 30^\circ$ off the boresight, and the phase shifts for the array elements related to spatial locations were $\xi_1 = 0, \xi_2 = 0.5\pi, \xi_3 = \pi, \dots, \xi_{16} = 8\pi$. They were parts of total phase change in each channel but were removed during calibration. In order to eliminate influence from path losses, which is out of scope of the study, the amplitude of the received signal A_m was assumed as 1.

In the process of calibration, at each iteration, the estimation on phase for the next iteration was calculated by using the estimated phase at the current iteration and an approximated gradient. The gradient was calculated following the description in Section 2.2. Once the phases for all element channels were determined, the combined signal V at the array output was calculated by

$$V = \mathbf{s} \cdot \mathbf{w}^T. \quad (25)$$

In searching for the optimal phase values for correction, $\hat{\boldsymbol{\tau}}_k$ was renewed at each iteration until the L_f satisfied the convergence condition. Three convergence conditions were used to examine the accuracy level when the convergence threshold was 0.1, 0.01, or 0.001, respectively.

The algorithm in the frequency domain was based on a single frequency; in order to investigate the wideband applicability of the algorithm, the performance of the array was evaluated by using the same set of approximated phase values for adjustment from 1 GHz at other two adjacent frequencies, 0.95 and 1.05 GHz. The phase shift vector, $\boldsymbol{\xi}$, and its component values were associated with the relative positions of array elements and were removed directly prior the first iteration as they were known by simple calculation. We applied $\boldsymbol{\psi}^*$, which was estimated by the algorithm at 1 GHz to the antenna array for receiving. The received power from the array output at 0.95 and 1.05 GHz were compared to an ideal case when the array were fully calibrated at these frequencies.

The phase shift related to the position for the m th channel, ξ_m , at 1 GHz can be calculated by

$$\begin{aligned} \xi_{1\text{GHz},m} &= 2\pi(m-1)d\sin\theta/\lambda_{1\text{GHz}} \\ &= 2\pi(m-1) \times 0.15 \times \frac{0.5}{0.3} \\ &= 0.5(m-1)\pi. \end{aligned} \quad (26)$$

The signal received by the m th element at 1 GHz can be expressed by

$$\mathbf{v}_{1\text{GHz},m} = e^{-i\xi_{1\text{GHz},m}} e^{-i[\gamma_m - \boldsymbol{\psi}_m^* - \xi_{1\text{GHz},m}]}. \quad (27)$$

At 0.95 GHz, the phase shift of the m th element due to the spatial position was

$$\begin{aligned} \xi_{0.95\text{GHz},m} &= 2\pi(m-1)d\sin\theta/\lambda_{0.95\text{GHz}} \\ &= 2\pi(m-1) \times 0.15 \times \frac{0.5}{\lambda_{1\text{GHz}}} \times \frac{\lambda_{1\text{GHz}}}{\lambda_{0.95\text{GHz}}} \\ &= 0.95 \times 0.5(m-1)\pi. \end{aligned} \quad (28)$$

The signal received by the m th element at 0.95 GHz after performing calibration using the estimated phase coefficient from the algorithm based on 1 GHz was

$$V_{0.95\text{GHz},m} = e^{-j\xi_{1\text{GHz},m}} e^{-j[\gamma_m - \psi_m^* - \xi_{0.95\text{GHz},m}]}. \quad (29)$$

The power at the array output was calculated by

$$P = \mathbb{E}\{|V|^2\}. \quad (30)$$

3.2 | Results for calibration in the frequency domain

The algorithm was run through without prior information on the random phase distortions mentioned in the last section. The loss function was established based on the combined power at the array output as defined in Equation (16) and compared against the convergence threshold at each iteration. The algorithm terminated once the condition was met. Figure 2a showed the performance of the algorithm with different convergence conditions. According to the definition of the loss function, the power of the combined signal after calibration reaches 90%, 99%, or 99.9% of the maximum

power available at the array output, with the convergence threshold set as 0.1, 0.01, or 0.001 accordingly.

The approximation errors for calibration can be represented by the difference between $[\gamma_1 \ \gamma_2 \ \dots \ \gamma_{16}]$ and $[\psi_1^* \ \psi_2^* \ \dots \ \psi_{16}^*]$, and they were illustrated in Figure 2b. While the convergence criteria was set as 0.001, the difference between the γ and ψ^* was less than 5° for all element channels, which were summarised in Table 2. The standard deviations of the approximation errors for these three scenarios have been calculated and listed in the Table 3. It is pointed out that while the $L_f \leq 0.001$, the standard deviation of the approximation errors was less than 2° .

Table 4 compared the performances of the calibrated array at 0.95 GHz, 1 GHz, and 1.05 GHz using calibration coefficients acquired through the algorithm at 1 GHz with the convergence threshold of 0.001. At 1 GHz, the received power from the calibrated array was close to 99.9% of the power received from an ideal array; however, it reduces by more than 30% at 0.95 and 1.05 GHz with the observed frequency only 50 MHz away from the frequency for calibration.

TABLE 2 Experimental results for the array with 16 elements calibrated in the frequency domain when $L_f \leq 0.001$

Intrinsic phase γ (degree)	Approximated phase ψ^* (degree)	Approximation error $\gamma - \psi^*$ (degree)
28.8656	26.1269	2.7387
59.3298	54.4826	4.8472
34.1426	31.3064	2.8362
86.7745	83.5487	3.2258
50.2198	49.3145	0.9053
14.3354	16.3981	-2.0627
44.9314	44.41	0.5214
39.6659	39.1846	0.4813
86.1213	84.4081	1.7132
48.478	44.112	4.366
8.2334	6.3999	1.8335
4.3258	3.4034	0.9224
36.3771	35.2541	1.123
78.2317	75.6992	2.5325
64.1999	65.1854	-0.9855
45.3267	43.5161	1.8106

TABLE 3 Standard deviation of approximation error when the convergence threshold is 0.1, 0.01, or 0.001 in the frequency domain

Convergence threshold	Standard deviation (degree)
0.1	15.0786
0.01	5.9257
0.001	1.7933

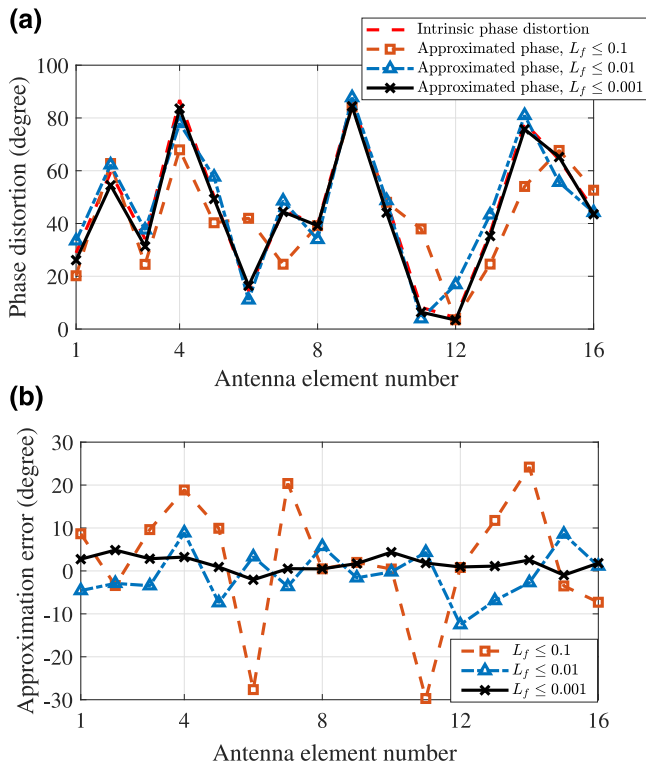


FIGURE 2 Approximated phase shift and approximation error when the convergence threshold is 0.1, 0.01, or 0.001, respectively, in the frequency domain. (a) Approximated and intrinsic phase distortion and (b) approximation error between the intrinsic and approximated phase shift

3.3 | The experiment in the time domain

A short pulse was used to implement the algorithm in the time domain. The array setting was the same as in the frequency domain where the total number of elements, $M = 16$ and the element spacing of $d = 0.15$ m. The coefficient constant was set as $a_t = 0.1L_t(k)/|\hat{\mathbf{g}}_k|$ where k was the iteration number, $L_t(k)$ was the loss function defined in Equation (22), and $\hat{\mathbf{g}}_k$ was the approximated gradient at the k th iteration, as defined in Section 2.3. Since the loss function was more susceptible than the one in the frequency domain, a_t was taken being proportional to the value of the loss function at each iteration for a successful convergence. Then c_t ($c_t = 0.1$) was determined using optimisation. The time delay distortions were generated randomly in the element channels and $\boldsymbol{\gamma} = [-0.7222, -0.3305, -0.9352, -0.3615, 0.3188, 0.2325, -0.4646, -0.7118, 0.1604, 0.6035, -0.1765, 0.4353, 0.2565, 0.4433, 0.5461, 0.2556]$ ns; the delay distortion for each element was in the range of $[-2, 2]$ ns and generated following the Gaussian distribution. At the beginning of the algorithm, the $\hat{\boldsymbol{\tau}}_0$, the vector representing the initial guess on the time delay distortions, was generated within the same time range and followed the same distribution. The pulse signal defined in Equation (17) had $\sigma_p^2 = 0.01$, which was assumed to be impinging on the array with the angle of arrival $\theta = 30^\circ$ off the boresight. c is the speed of light, the time delay for the element m due to relative separation to the reference element, $\xi_m = (m - 1)d\sin\theta/c$, and then $\xi_1 = 0, \xi_2 = 0.25, \dots$, and $\xi_{16} = 4$ ns. The peak of the pulse signal was set as 1, so the peak amplitude of the combined pulse signal at the array output was 16 when the receiving condition was ideal, and after the P_k was measured at the array output, R_k and C_k were computed based on Equations (23) and (24), respectively.

The \mathbf{s}_k and \mathbf{s}_{peak} were sampled in the time range between -2 and 2 ns with a sampling interval of 0.01 ns, resulting in the total number of samples in the pulse signals mentioned in Equation (24) being $401, N = 401$ Equation (24).

The algorithm loops terminated when the convergence condition was met, and three thresholds were used for comparison with $0.2, 0.1, \text{ or } 0.01$, respectively. The vector $\hat{\boldsymbol{\tau}}_k$ was acquired when the algorithm stopped, and then we had $\boldsymbol{\tau}^* = \hat{\boldsymbol{\tau}}_k$ which was the vector used for calibration. The vector $\boldsymbol{\xi}$ representing fixed time delays related to the array configuration, was known once the frequency and the array pitch were decided, and they were excluded from the optimisation process. From the algorithm output, $\boldsymbol{\tau}^*$ was obtained and the values were used to make compensation for the random time

TABLE 4 The power and the ratio to maximum power at 0.95 GHz, 1 GHz, or 1.05 GHz in the frequency domain, using the frequency of 1 GHz for calibration, and convergence threshold is 0.001

Frequency (GHz)	Ideal power (W)	Power after cal. (W)	Power ratio (%)
0.95	256	171.1367	66.8503
1	256	255.7501	99.9024
1.05	256	168.3131	65.7473

delays, $\boldsymbol{\gamma}$, introduced at the beginning of the experiment. The performance of the algorithm was evaluated by comparing the resolved time delays with the intrinsic time delays generated randomly in the element channels.

3.4 | Results for calibration in the time domain

The resolved time delays from the algorithm were compared with the intrinsic time delays randomly generated in the channels and they are shown in Figure 3a. The algorithm was run with three convergence conditions of $L_t \leq 0.2, L_t \leq 0.1$ or $L_t \leq 0.01$ respectively. The agreement becomes better when the convergence condition became more stringent. The power of combined signal at the array output after being calibrated was more than 80%, 90%, or 99% of the maximum power for ideal receiving condition when the convergence threshold was equal to 0.2, 0.1, or 0.01, respectively.

The approximation errors of the algorithm were evaluated by the difference between $[\gamma_1, \gamma_2, \dots, \gamma_M]$ and $[\tau_1^*, \tau_2^*, \dots, \tau_M^*]$, and this was depicted in Figure 3b for all 16 channels. With the convergence condition using $L_t \leq 0.01$, the random time delays, the resolved time delays from the algorithm, and their differences were summarised in Table 5. With three different convergence criteria, the standard deviation of the approximation errors for these three scenarios were compared in

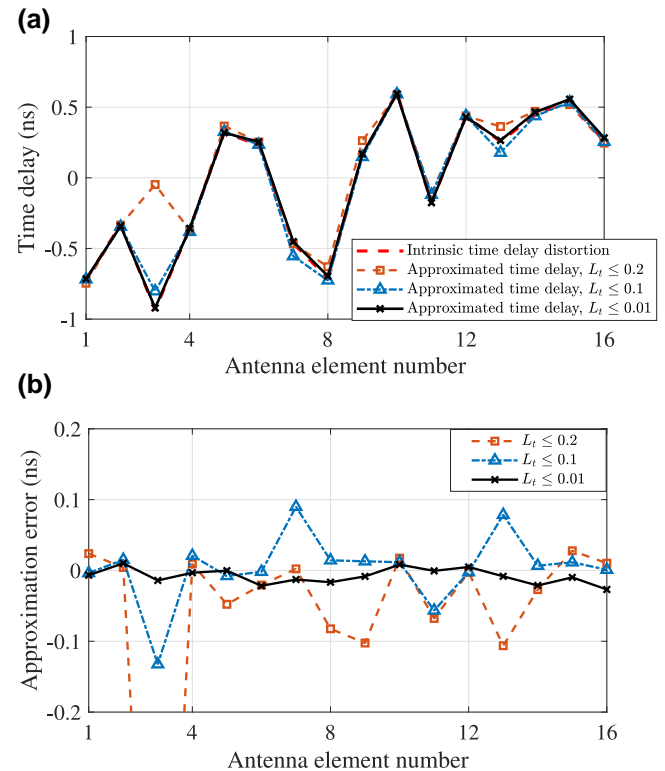


FIGURE 3 Approximated time delay and approximation error in the time domain when the convergence threshold is 0.2, 0.1 or 0.01.

(a) Approximated and intrinsic time delay distortion and (b) approximation error between the approximated and intrinsic time delay distortion

TABLE 5 Experimental results for the array with 16 elements calibrated in the time domain when convergence threshold is 0.01

Intrinsic time delay γ (ns)	Approximated time delay τ^* (ns)	Approximation error $\gamma - \tau^*$ (ns)
-0.7222	-0.7155	-0.0067
-0.3305	-0.3406	0.0101
-0.9352	-0.9211	-0.0141
-0.3615	-0.3583	-0.0032
0.3188	0.3191	-0.0003
0.2325	0.2542	-0.0217
-0.4646	-0.4518	-0.0128
-0.7118	-0.6952	-0.0166
0.1604	0.1688	-0.0084
0.6035	0.5953	0.0082
-0.1765	-0.1759	-0.0006
0.4353	0.4304	0.0049
0.2565	0.2648	-0.0083
0.4433	0.4645	-0.0212
0.5461	0.5559	-0.0098
0.2556	0.2825	-0.0269

Table 6. When $L_t \leq 0.01$, the standard deviation of the approximation errors were close to 0.01 ns.

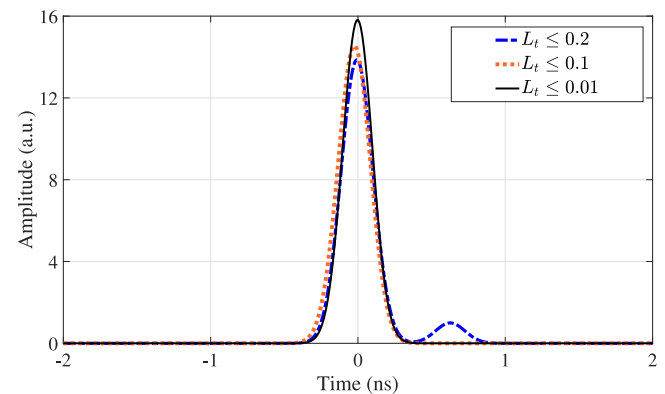
The combined signals after calibration with the three different convergence conditions were plotted in Figure 4. It is noted that under a perfect receiving condition where all element channels were fully synchronised, the peak of the pulse signal for each element is 1, so the peak amplitude of combined pulse signal is expected to be 16. From the numerical experiment, the peak amplitude of the combined signal after calibration with $L_t \leq 0.01$ was close to 16. This verified the effectiveness of the algorithm implemented in the time domain. In Table 7, the performance of the proposed method was compared with other existing calibration methods where a perturbation technique was involved. The benefit of the proposed method was clearly seen for calibrating antenna arrays with ultrawide bandwidth.

4 | DISCUSSION

The SPSA algorithm becomes popular in solving multivariate random search problems. It is attractive as it requires only two function measurements at each iteration step, and convergence is guaranteed with a reasonably simple computation. It appears promising for antenna array calibration. A calibration method based on simultaneous perturbation on multiple channels is established and is applicable in both frequency and time domains. Unlike traditional calibration methods that carry out phase probing and adaptation in a sequence, this method is

TABLE 6 Standard deviation of the approximation error when the convergence threshold is 0.2, 0.1, or 0.01 in the time domain

Convergence threshold	Standard deviation (ns)
0.2	0.2203
0.1	0.0491
0.01	0.0108

**FIGURE 4** Signals at array output after calibration when the convergence threshold is 0.2, 0.1, or 0.01, respectively**TABLE 7** Comparison of calibration methods using a perturbation technique

Method	Domain	Measurements
[18, 31]	FD	94,208
[19]	FD	93,184
[20, 27]	FD	61,440
[28]	FD	33,792
[32, 33]	FD	16,384
[34]	FD	122,880
This work	TD	1011 (200 runs)

Note: The number of elements in the array was 16, and 1024 frequency points were assumed to be calibrated when the calibration was implemented in the frequency domain.

particularly efficient because random perturbations are applied to all channels simultaneously. During the search for the optimal coefficients, only two measurements were required at each update step, which greatly reduces the time taken for calibration.

In both implementations, we observed that the frequency-domain calibration performs more conveniently for narrow band systems as it can be implemented with only two power measurements in each iteration. However, for systems of a broad frequency bandwidth, calibration needs to be done in a sequence at each frequency point over the entire band, which is inefficient and time-consuming given a large number of frequency points. On the other hand, the time-domain calibration exhibits its novelty for array calibration, along with a high performance in wideband antenna arrays. Both of these

methods will be of significant contribution on the calibration of wideband and large-scale phased antenna arrays, which is promising in smart antenna and contemporary satellite communication.

It is worth mentioning that the time width of the pulse signal used in the calibration process is dependent on the frequency bandwidth of the antenna arrays to be calibrated, which in turn is closely related to the time delay spread in each element channel. For example, in the time domain calibration experiment, the time width of the pulse signal for calibration was 1 ns, and the time delay distortion in each element channel was distributed in the range between -1 ns and $+1$ ns. The frequency bandwidth of the short pulse for calibration is 930 MHz (3 dB bandwidth from the peak of the frequency spectrum), and this corresponds to an approximate time width of 1 ns for the pulse signal in the time domain. When the antenna array has a greater bandwidth, a narrower pulse signal may be adopted. The experimental results have shown that a successful convergence of the proposed method relies on three key parameters: the pulse signal with a suitable time duration; the initially chosen values of a_f and c_f in the frequency domain; and the correct choice of values for a_t and c_t if implemented in the time domain. For the time domain implementation, the value of a_t varies with iterations.

5 | CONCLUSION

A method for antenna array calibration based on the SPSA algorithm was proposed, which can be adopted both in frequency and time domains. The distinct advantage of the method compared to other existing approaches was that it achieved the optimal objective values of multiple variables for calibration through simultaneous perturbation instead of in a sequence, and a high performance efficiency was exhibited. Simulation experiments confirmed its effectiveness for calibrating arrays with random phase or time delay distortions due to environment or sensitive active devices. It was highly efficient for extracting calibration coefficients in both frequency and time domains as the perturbations were applied in element channels simultaneously in conjuncture with stringent conditions to reach convergence. The successful implementation in the time domain demonstrated that the method can be applied efficiently to calibrate antenna arrays of ultrawide bandwidth.

AUTHOR CONTRIBUTIONS

Huijuan Xing: Investigation, Methodology, Software, Validation, Writing – original draft. **Yongwei Zhang:** Conceptualization, Funding acquisition, Supervision, Writing – review & editing. **Yanwei Fu:** Writing – review & editing. **Xianyang Lv:** Writing – review & editing. **Zhihuo Xu:** Writing – review & editing. **Jiajia Shi:** Writing – review & editing. **Quan Shi:** Writing – review & editing. **Murat Temiz:** Writing – review & editing. **Ahmed El-Makadema:** Writing – review & editing.

ACKNOWLEDGEMENTS

This work was supported in part by the NSFC under Grants 62174091 and 62201294, in part by Post-Doc International Exchange Programme YJ20210098, and in part by the Post-graduate Research & Practice Innovation Program of School of Transportation and Civil Engineering, Nantong University (NTUJTXYG12201).

CONFLICT OF INTEREST

The author declares that there is no conflict of interest that could be perceived as prejudicing the impartiality of the research reported.

DATA AVAILABILITY STATEMENT

Data sharing is not applicable to this article as no new data were created or analysed in this study.

ORCID

Huijuan Xing  <https://orcid.org/0000-0001-9824-7017>

Yongwei Zhang  <https://orcid.org/0000-0001-9201-4511>

Yanwei Fu  <https://orcid.org/0000-0003-0272-7302>

REFERENCES

1. Roh, W., et al.: Millimeter-wave beamforming as an enabling technology for 5G cellular communications: theoretical feasibility and prototype results. *IEEE Commun. Mag.* 52(2), 106–113 (2014). <https://doi.org/10.1109/mcom.2014.6736750>
2. Temiz, M., et al.: On the impact of antenna array geometry on indoor wideband massive MIMO networks. *IEEE Trans. Antennas Propag.* 69(1), 406–416 (2021). <https://doi.org/10.1109/tap.2020.3008662>
3. Helander, J., et al.: Performance analysis of millimeter-wave phased array antennas in cellular handsets. *IEEE Antennas Wirel. Propag. Lett.* 15, 504–507 (2016). <https://doi.org/10.1109/lawp.2015.2455040>
4. Moon, T., Gaun, J., Hassanieh, H.: Know your channel first, then calibrate your mmWave phased array. *IEEE Des. Test.* 37(4), 42–51 (2020). <https://doi.org/10.1109/mdat.2020.2968286>
5. Tyler, N., Allen, B., Aghvami, H.: Adaptive antennas: the calibration problem. *IEEE Commun. Mag.* 42(12), 114–122 (2004). <https://doi.org/10.1109/mcom.2004.1367563>
6. Tyler, N., Allen, B., Hamid, A.: Smart antenna calibration: requirements and techniques. *IET Semin. Dig.*, 1–3 (2005)
7. Schuss, J., et al.: Large-scale phased array calibration. *IEEE Trans. Antennas Propag.* 67(9), 5919–5933 (2019). <https://doi.org/10.1109/tap.2019.2920231>
8. Mano, S., Katagi, T.: A method for measuring amplitude and phase of each radiating element of a phased array antenna. *Electron. Commun. Jpn.* 65-B(5), 58–64 (1982). <https://doi.org/10.1002/ecja.4410650508>
9. Yonezawa, R., et al.: Beam-shape correction in deployable phased arrays. *IEEE Trans. Antennas Propag.* 47(3), 482–486 (1999). <https://doi.org/10.1109/8.768783>
10. Yoon, H.-J., Min, B.-W.: Improved rotating-element electric-field vector method for fast far-field phased array calibration. *IEEE Trans. Antennas Propag.* 69(11), 8021–8026 (2021). <https://doi.org/10.1109/tap.2021.3083796>
11. Aumann, H.M., Fenn, A.J., Willwerth, F.G.: Phased array antenna calibration and pattern prediction using mutual coupling measurements. *IEEE Trans. Antennas Propag.* 37(7), 844–850 (1989). <https://doi.org/10.1109/8.29378>
12. Zhang, X., et al.: Effective mutual coupling estimation and calibration for conformal arrays based on pattern perturbation. *IET Microw. Antennas Propag.* 14(15), 1998–2006 (2020). <https://doi.org/10.1049/iet-map.2019.0750>

13. Bao, J., et al.: An improved method for mutual coupling calibration with application in wide-angle direction-of-arrival estimations. *Electromagnetics*. 35(2), 101–111 (2015). <https://doi.org/10.1080/02726343.2014.987638>
14. Zhang, D., et al.: A subspace-based channel calibration algorithm for geosynchronous satellite-airborne bistatic multi-channel radars. *IET Radar. Sonar Navig.* 8(9), 1008–1017 (2014). <https://doi.org/10.1049/iet-rsn.2013.0325>
15. Nafe, A., et al.: An in-situ self-test and self-calibration technique utilizing antenna mutual coupling for 5G multi-beam TRX phased arrays. In: *IEEE MTT-S Int Microwave Symp*, 1229–1232 (2019)
16. Kim, K.S., Yang, E., Myung, N.H.: Self-calibration of an active uniform linear array using phase gradient characteristics. *IEEE Antennas Wirel. Propag. Lett.* 18(3), 497–501 (2019). <https://doi.org/10.1109/lawp.2019.2895268>
17. Chae, S.-C., et al.: Coupler integrated microstrip patch linear phased array for self-calibration. *IEEE Antennas Wirel. Propag. Lett.* 19(9), 1615–1619 (2020). <https://doi.org/10.1109/lawp.2020.3011862>
18. Leavitt, M.: A phase adaptation algorithm. *IEEE Trans. Antennas Propag.* 24(5), 754–756 (1976). <https://doi.org/10.1109/tap.1976.1141404>
19. Djigan, V.I., Kurganov, V.V.: Antenna array calibration algorithm without access to channel Signals. *Radioelectron. Commun. Syst.* 63(1), 1–14 (2020). <https://doi.org/10.3103/s073527272001001x>
20. Sorace, R.: Phased array calibration. *IEEE Trans. Antennas Propag.* 49(4), 517–525 (2001). <https://doi.org/10.1109/8.923310>
21. Cantoni, A.: Application of orthogonal perturbation sequences to adaptive beamforming. *IEEE Trans. Antennas Propag.* 28(2), 191–202 (1980). <https://doi.org/10.1109/tap.1980.1142299>
22. Godara, L.C.: Improved LMS algorithm for adaptive beamforming. *IEEE Trans. Antennas Propag.* 38(10), 1631–1635 (1990). <https://doi.org/10.1109/8.59777>
23. Spall, J.C.: Multivariate stochastic approximation using a simultaneous perturbation gradient approximation. *IEEE Trans. Autom. Control.* 37(3), 332–341 (1992). <https://doi.org/10.1109/9.119632>
24. Spall, J.C.: Implementation of the simultaneous perturbation algorithm for stochastic optimization. *IEEE Trans. Aerosp. Electron. Syst.* 34(3), 817–823 (1998). <https://doi.org/10.1109/7.705889>
25. Spall, J.C.: An overview of the simultaneous perturbation method for efficient optimization. *Johns Hopkins APL Tech. Dig.* 19(4), 482–492 (1998)
26. Spall, J.C.: Adaptive stochastic approximation by the simultaneous perturbation method. *IEEE Trans. Autom. Control.* 45(10), 1839–1853 (2000). <https://doi.org/10.1109/tac.2000.880982>
27. Wang, H., Sun, H.: Phased array antenna quick calibration method. *J. Beijing Univ. Aeronaut. Astronaut.* 42(12), 2709–2714 (2016). <https://doi.org/10.13700/j.bh.1001-5965.2015.0828>
28. Long, R., et al.: Fast amplitude-only measurement method for phased array calibration. *IEEE Trans. Antennas Propag.* 65(4), 1815–1822 (2017). <https://doi.org/10.1109/tap.2016.2629467>
29. Ljung, L.: Analysis of recursive stochastic algorithms. *IEEE Trans. Autom. Control.* 22(4), 551–575 (1977). <https://doi.org/10.1109/tac.1977.1101561>
30. Fakharzadeh, M., et al.: Zero-knowledge beamforming of phased array antennas based on simultaneous perturbation gradient approximation. In: *IEEE Antennas Propag. Soc. AP-S Int. Symp*, 537–540 (2006)
31. Steyskal, H., Shore, R., Haupt, R.: Methods for null control and their effects on the radiation pattern. *IEEE Trans. Antennas Propag.* 34(3), 404–409 (1986). <https://doi.org/10.1109/tap.1986.1143816>
32. Lee, K.-M., Chu, R.-S., Liu, S.-C.: A built-in performance-monitoring/fault isolation and correction (PM/FIC) system for active phased-array antennas. *IEEE Trans. Antennas Propag.* 41(11), 1530–1540 (1993). <https://doi.org/10.1109/8.267353>
33. Hampson, G.A., Smolders, A.B.: A fast and accurate scheme for calibration of active phased-array antennas. In: *IEEE Antennas Propag. Soc. Int. Symp: Wirel. Technol. Inf. Netw, APS-Held Conjunction USNC/URSI National Radio Sci. Meet*, 2, 1040–1043 (1999)
34. Takahashi, T., et al.: Fast measurement technique for phased array calibration. *IEEE Trans. Antennas Propag.* 56(7), 1888–1899 (2008). <https://doi.org/10.1109/tap.2008.924682>
35. Hussain, M.G.M.: Theory and analysis of adaptive cylindrical array antenna for ultrawideband wireless communications. *IEEE Transactions Wirel. Commun.* 4(6), 3075–3083 (2005). <https://doi.org/10.1109/twc.2005.857995>

How to cite this article: Xing, H., et al.: Antenna array Calibration methods based on simultaneous perturbation. *IET Microw. Antennas Propag.* 16(14), 898–909 (2022). <https://doi.org/10.1049/mia2.12304>